Preparing Master Grooves for Lapping Discs Used in Micromachining of VideoDisc Styli

W. R. Roach and I. Gorog
RCA Laboratories, Princeton, NJ 08540

Abstract—The tip of a long playing VideoDisc stylus has a shape resembling a keel of microscopic dimensions. The machining of such a keel shape on the faceted tip of a diamond log requires a lapping disc having an approximately 4.5-μm deep, 2.4-μm-wide groove of minimal taper. The method of generating a photoresist master having a groove of this geometry by laser exposure and development is described. Details of a laser recording system for the production of a uniform lapping groove over a 3-inch-wide band on a 12-inch-diameter disc and methods for evaluating the groove profile are presented. A general theory of the exposure/development process is used to generate a family of groove profiles that traces the evolution of the groove shape during photoresist development. This theory provides a qualitative framework for establishing optimum exposure/development conditions.

1. Introduction

The RCA VideoDisc recording is played using a diamond stylus whose tip is precisely shaped so as to ride smoothly in the 140-degree V-shaped groove. The trailing vertical surface of the stylus carries an electrode that capacitively senses the presence of signal elements on the vinyl disc. The stylus extends the full width of the groove so that the signal-to-noise performance on playback is maximized. The stylus might thus be configured as shown in Fig. 1. However, after extensive use, such a stylus would wear causing the width of the tip to broaden, which would eventually result in the configuration shown in Fig. 2. During playback such a stylus could pick up unwanted signals from the adjacent grooves. It could also

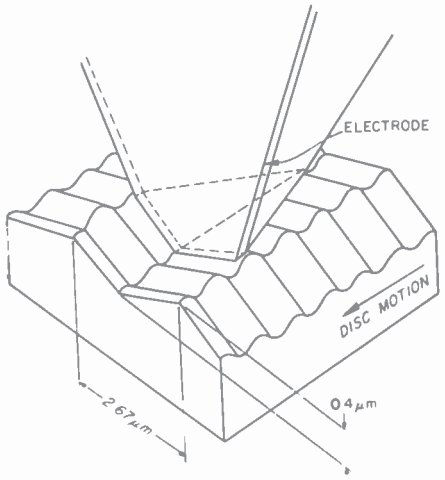

Fig. 1—View of faceted stylus in RCA VideoDisc groove.

lose the wanted signal because minor groove-pitch nonuniformities could cause the tip to not conform precisely to this extended profile for many of the grooves on the disc. It was suggested by E. O. Keizer[1] that both problems could be avoided by shaping the stylus tip as indicated in Fig. 3. With such a configuration, the stylus tip width will not vary during life, and thus it will consistently ride in and sense signals from a single groove.

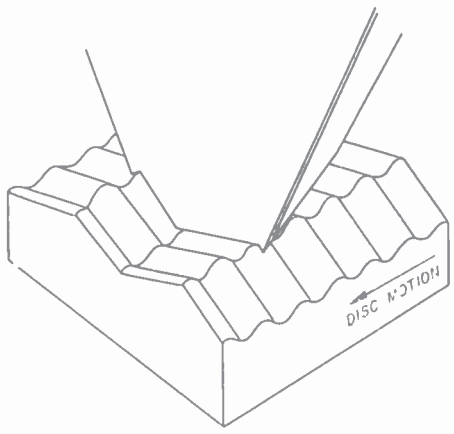

Fig. 2—Effect of wear on improperly shaped stylus showing electrode overlap to adjacent grooves.

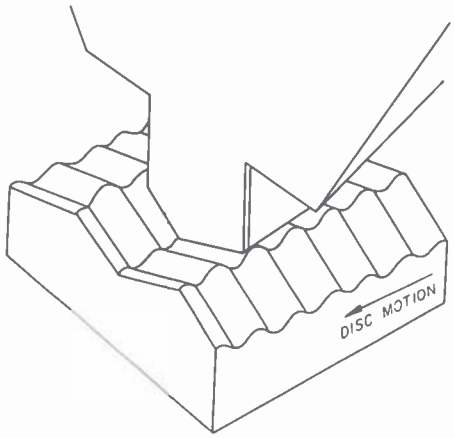

Fig. 3—View of ideal keel-lapped stylus tip riding in VideoDisc groove.

The production process for a Video-Disc diamond stylus with a tip geometry approaching that of Fig. 3 includes a machining operation that shapes the electroded and faceted tip by lapping it into a spiral groove of precisely shaped profile. The required profile of the keel-lapping groove is relatively narrow (2.4 μm wide) and deep (4.5 μm deep). Because of the large aspect ratio, both the production of the original groove and its replication to form the final lapping discs are relatively difficult. As indicated in Fig. 3, the ideal keel-lapped stylus would have vertical walls, but in practice it is impractical, if not impossible, to replicate lapping discs unless the walls have some taper. Taper is necessary because, during replication of the lapping disc, a reentrant structure will form an interlocking system with the next generation part, and the two cannot be separated without damaging them. However, too much taper would reduce the effectiveness of the resultant keel-lapped shape. A good compromise is to accept a 2.5° outward tilt of the groove walls, as indicated in Fig. 4. The groove must also be symmetrical to produce a keel whose prow is properly centered for optimum tracking performance. The groove pitch on the master recording used to make the lapping discs should be constant so that the lapping station can be set up with a constant pitch drive. The groove spacing should be large enough to insure that the shoulders of the fully keel-lapped tip are flat. The maximum number of turns per disc is desirable, consistent with the shoulder-width requirement, so that the largest possible number of stylii can be lapped on a given disc. This requirement is adequately met by a 9-μm groove period.

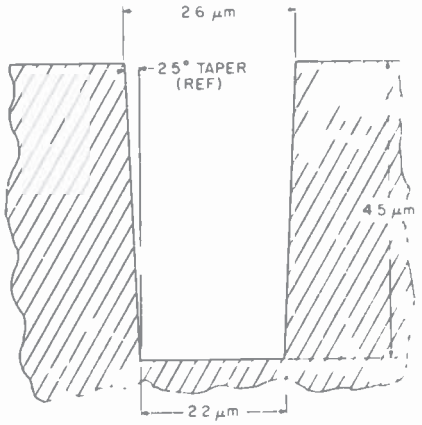

Fig. 4—Groove profile required for keel-lapping master.

The keel-lapping process is typically followed by a very short lap of the stylus on another spiral-grooved disc on which the grooves have the same V-shaped profile as the production VideoDiscs (140° included angle) to insure that no wear-in time is necessary to reach the maximum electrical output from a new stylus.

This paper outlines the method used to generate the master part used in the production of lapping discs, provides details of the optical recording system used to generate grooves with a uniform profile over a 3-inch-wide band of approximately one-foot outside diameter, describes the special measurement techniques that have been developed to evaluate the resultant groove shape, and discusses a theoretical model used to gain insight into the optical recording/development process.

2. Keel-Lap Mastering

The technique used to generate the metal keel-lap master consists of the following steps:

(a) coating a large-diameter copper-plated aluminum substrate with a uniform layer of photoresist,
(b) baking the resist to drive off the solvent,
(c) exposing a spiral track with a focused laser beam,
(d) developing the resist to remove exposed photoresist down to the substrate,
(e) washing off the developer and drying the resist,

(f) coating the deep relief surface with a thin conductive layer, and (g) electroplating the nickel to form the metal master.

Of these steps, this paper discusses in detail only (c) keel-lap recording and (d) photoresist developing. These two aspects are not only central to the production of the keel-lap master but also have wider applicability in the production of any system where deep and narrow grooves of controlled profile are required on a large diameter substrate.

There is one other crucial step in the process of obtaining a suitable master, and that is to evaluate the geometry of the grooves actually produced and, using this information as feedback, to improve the choice of recording/developing conditions for subsequent recordings. Because of the dimensions involved, only a scanning electron microscope (SEM) has the resolution necessary to characterize the groove profile adequately. Unfortunately, all processes that we are aware of to prepare samples for accurate SEM evaluation of the deep-grooved recording profile are destructive of the part involved. Also, when the original nickel master is pulled off the substrate, the parting takes place in the resist, resulting in damage to the relief pattern. Thus, only one electroform nickel part (metal master) can be made directly from the photoresist-covered substrate. If we want to evaluate a possibly useful recording (one that might actually be utilized for the production of lapping discs) we must generate from the master a part that can be sacrificed. In our case we are forced to generate from the production master a mold, which is then used to make several stampers. Of these, the first and second stampers are reserved for further fanout, since they are the best. The third and fourth stampers are used to press test lapping discs. Therefore, the fifth stamper is the first available for groove-profile evaluation. This multiple replication procedure in itself takes several days, and the groove-profile evaluation several more. Even then we have gained information on only one set of recording/developing conditions.

To reduce our dependence on this lengthy full-fanout feedback, we have devised an alternative method involving the production of a group of six identically coated substrates and the recording of as many as 20 separate test bands on one or two of these substrates, followed by immediate groove profile evaluation of thin electroform metal masters. Information from these test recordings can be used to establish conditions for recording the remaining members of the set, provided that this set of substrates has resist layers that are matched in thickness to within 0.2 μm. By this method we can make

two test recordings, evaluate their groove shapes, and record the remaining four members of the set as production masters, all within approximately three weeks. The four production masters can then be fanned out and evaluated at leisure while another complete set is in process.

Processing steps that cause modifications of the laser-recorded groove profile have also been developed, but these are beyond the scope of this paper.

3. Keel-Lap Recording Requirements

The recording of the keel-lapping grooves involves laser exposure of a spiral track in a photoresist layer that is coated onto a flat, 1/2-inch thick, 14-inch diameter, copper-plated, aluminum substrate. The thickness of the photoresist is approximately 4.5 μm with a uniformity of ±0.1 μm over the band from 2.8- to 5.8-inch radius. The resist used is a positive-developing RCA proprietary compound. The RCA formulation is used to insure complete quality control over the composition. The resist thickness must be maintained within the limits specified, since the exposure/development process produces a groove whose depth is the resist thickness and whose profile is a complicated function of the resist thickness, beam power, beam shape, focus position, substrate reflectivity, and development parameters.

The function of the keel-lap recorder then is to provide a laser beam that is focused in the photoresist at a fixed height above the copper–photoresist interface and scanned along a spiral track on the substrate. This height must be controlled to better than ±6% of the film thickness to insure a uniform groove shape. To maintain as many parameters constant as possible during the recording of production masters, these recordings are typically made at a constant laser power with a constant linear velocity of the substrate under the beam. The recording time was chosen to be 1/2 hour. To scan the approximately 500 cm^2 area during this time, the required linear velocity of the beam over the substrate surface is 300 cm/sec. It is fortunate that at this scan velocity, a moderate power He-Cd laser causes a large increase in the solubility of the exposed regions of the photoresist in the developer without simultaneously causing significant bleaching at the 4416 Å wavelength. It is essential to maintain a strong absorption in the resist throughout the exposure process if we are to obtain the optimum groove shape.

4. Keel-Lap Recorder

The system that has been used for recording masters of a uniformity adequate for mass production of keel-lapped styli is similar to that described by A. H. Firester et al[2] for optically reading VideoDisc substrates. The keel-lapping recorder is shown in Fig. 5. Every RCA stylus that has been sold has a keel lapped tip whose profile is traceable to an optical master generated on this machine.

4.1 Beam Forming Optics

The major components of the optical system necessary for the generation of the keel-lap masters are shown in Fig. 6. The 1-mm diameter beam from a 20-mW helium-cadmium laser is directed through a polarizer, quarter-wave plate, and a beamsplitter. Distortions in the beam profile introduced by these elements are reduced by passing the beam through a $\times 5$ microscope objective and a 25-μm pinhole. To produce our smallest diameter beam in the photoresist we next insert a 150-mm focal-length lens positioned a focal length away from the pinhole to recollimate the beam. Next a beam-limiting aperture (7.6 mm in diameter in this case) is used

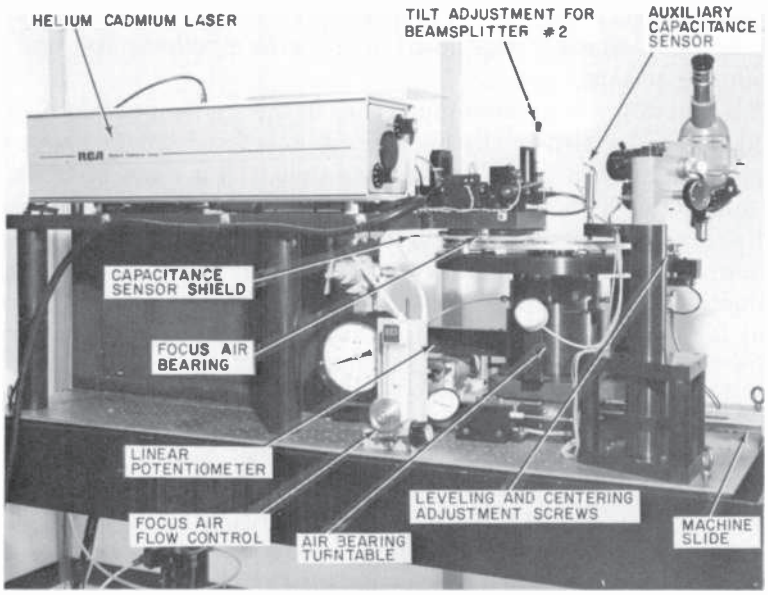

Fig. 5—View of optical keel-lap recorder.

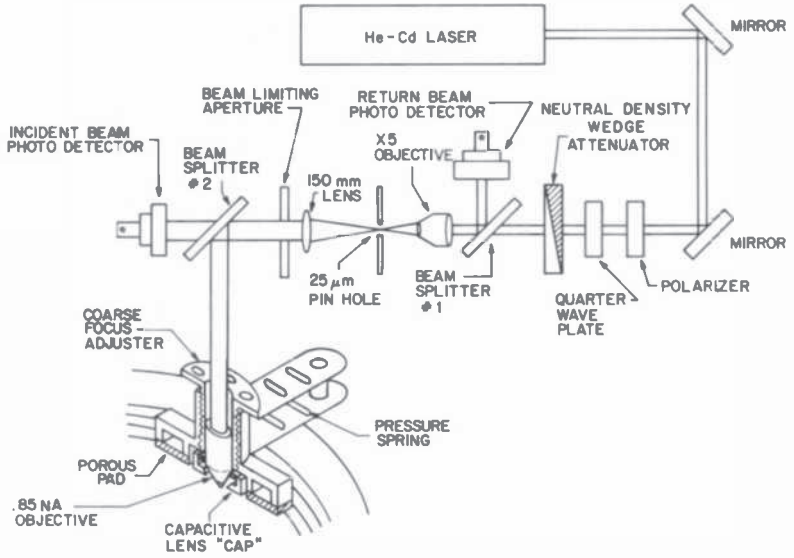

Fig. 6—Schematic of keel-lap-recorder optics.

to block all but the central portion of the Airy ring pattern[3] generated by diffraction from the pinhole.

With the Airy rings thus removed, the beam profile is approximately Gaussian. For a Gaussian profile, the power distribution $I(\rho)$ as a function of radius ρ is

$$I(\rho) = I(O) \exp(-\rho^2/w_p^2), \quad [1]$$

where $I(O)$ is the power on the optical axis and w_p is the Gaussian (power) parameter. The diameter of the beam at which $I(\rho)$ is just $1/2$ of $I(O)$ (defined as the full width at half maximum, FWHM) is

$$\text{FWHM} = 2w_p \sqrt{-\ln(0.5)} = 1.665\, w_p. \quad [2]$$

For the cylindrical Gaussian beam, this FWHM diameter also contains half the total power in the beam.

The collimated apertured beam (3.4-mm FWHM) is reflected off the beam splitter and passes through the final focusing objective (a $\times 50$, 0.85 NA, Leitz microscope objective with an input aperture of 8 mm) to produce a focused beam in the photoresist. When the objective is thus operated unfilled, with a small-diameter approximately Gaussian beam as input, it produces in the photoresist a focused beam that is also very nearly Gaussian. Under these conditions of illumination, although the spot diameter is larger than that attainable under uniform illumination of the focusing objec-

tive, the rings in the diffraction pattern are attenuated (in power) by a factor of approximately 100 as compared to those produced by a uniformly illuminated aperture.[4]

A measurement of the spot diameter at focus was made using the knife-edge scan technique described by Firester et al.[2] The result of this scan is shown in Fig. 7, where the downward displacement along the S-shaped curve represents increasing light intensity passed by the knife edge as it is removed from the beam. The horizontal axis is time, which can be related to distance by using the auxiliary sinusoidal signal, which is also shown. This auxiliary signal is the output from a He-Ne laser-illuminated Michelson interferometer that has one end mirror mechanically driven by the knife-edge motion. One complete cycle of the sinewave corresponds to one-half-wavelength (0.3164 μm) displacement of the knife edge.

For the exposure of the grooves to be uniform around the disc, the objective must be maintained at a fixed height (to within ± 1700 Å) above the photoresist surface while the substrate is rotated and translated under it at a scan velocity of several hundred cm/sec. To maintain focus to this accuracy, the final focusing objective is supported by a focus air bearing[2] consisting of two porous pads epoxied into aluminum cups. A 60-psi supply of filtered air is bled through a needle valve into the resulting chambers. This air exits downward through the pads and causes the structure supporting the lens to be lifted against a spring pressure and to ride a few mils above the resist surface. Very fine control of the air flow through these pads permits maintenance of the focus position to the required tolerance while the substrate is being rotated under the beam.

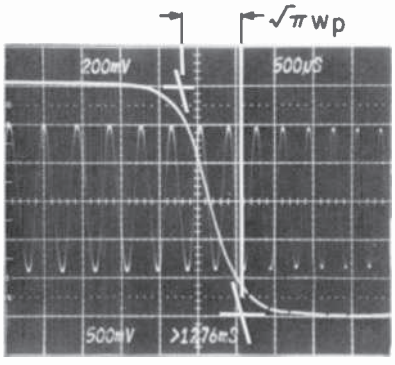

Fig. 7—Knife-edge spot size measurement. Downward deflection indicates increased light intensity. Sinusoidal interferometer peak spacing is 0.3164-μm knife-edge displacement.

4.2 Capacitance Sensor

To monitor the vertical position of the lens relative to the substrate, the final focusing objective was fitted with an aluminum cap. The flat ring-shaped bottom surface of the cap typically rides ~75 μm above the substrate surface, and the capacitance between the two surfaces (typically ~20 pF) varies as the reciprocal of the distance between them. Since the groove profile in the 4.5-μm thick resist must be substantially constant, the focal-plane position in the resist must not shift during the recording by more than ±0.3 μm. Refraction in the resist (see Sec. 4) requires that the lens height be maintained to within ±0.17 μm, corresponding to changes in lens-cap-to-substrate capacitance of ±0.05 pF. Since the stray capacitance associated with the lens cap, leads, etc., is ~25 pF, we require a system that will accurately measure changes of ±0.05 pF out of 45 pF. A capacitance bridge feeding a digital voltmeter provides a measure of the position to better than this precision, but such a system provides no absolute indication of where the lens focal plane is located. To establish the absolute scale for the capacitance sensor, we employ the optical-focus sensor described below.

4.3 Optical-Focus Sensor

The optical-focus sensor utilizes the recording beam after it has been reflected off the substrate. This return beam passes backward through the focusing objective, beam-splitter No. 2, beam-limiting aperture, collimating lens, pinhole, and microscope objective to beam-splitter No. 1 and the return-beam photodetector. The primary path of the laser beam is through the photoresist, followed by a reflection off the photoresist–substrate interface and back through the photoresist. The return-beam power as a function of focal position has one local maximum when the laser beam is focused at the photoresist-substrate surface. Another local maximum occurs in the return beam when the final objective has been raised sufficiently that the beam waist occurs at the upper surface of the resist. In this case, a small portion of the incident beam is reflected off the upper resist surface and is recollimated by the final focusing objective and passed backward along the optical path.

The positions of these two peaks on a return-beam-power-versus-capacitance plot establish the absolute scale for the capacitance sensor. Once the capacitance values corresponding to both top-surface focus and bottom-surface focus are established, an intermediate position can be maintained by controlling the capacitance reading

at the appropriate intermediate capacitance value. If the resist thickness of the production substrate is the same as that of the test substrate, the focus for the production recording can be made by setting the system up to have the same capacitance as that observed to give the best grooves on the test substrate. The response of the return-beam power to changes in lens height, as measured by the capacitance sensor, is shown in Fig. 8 for the case of a bare copper substrate. Note the well defined focus position.

4.4 Optical Behavior of Photoresist

When through-focus measurements of return-beam power versus capacitance are made on a photoresist-covered substrate, care must be taken to account for the possibility of bleaching the resist during the measurements. The results of a set of through-focus measure-

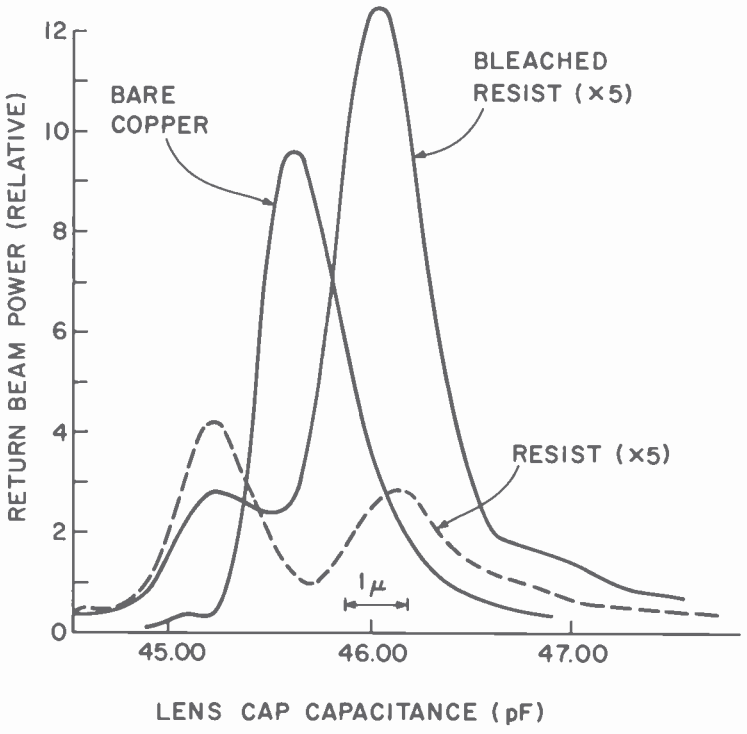

Fig. 8—Response of focus sensor versus lens cap capacitance. For approximate calibration, length of arrow represents 1-μm change in lens cap elevation.

ments of return-beam power are also shown in Fig. 8. Note, however, that the photoresist data is displayed with the vertical scale magnified by a factor of 5. In these measurements, the power in the focused laser beam was fixed at approximately 0.5 mW and the linear velocity of the substrate under the beam was varied. The bleached condition was obtained by allowing the beam to write over the same circular track at 325 cm/sec for several minutes. This bleached circular track was further probed by making scans of the return beam versus focal position at various surface velocities. Down to 2 cm/sec, these all produced essentially identical traces. Resist physical damage can occur for very slow scans (less than 10 cm/sec) for an input power of only 2 mW.

Note in Fig. 8 the two distinct peaks corresponding to focus at the air–photoresist interface and at the photoresist–copper interface. The vertical displacement of the lens necessary to shift the focal plane from the top surface to the photoresist–copper interface can be calculated as follows. The photoresist index of refraction n(resist) is given[5] as a function of the free-space wavelength of light, λ_0, by

$$n(\text{resist}) = 1.539 + \frac{0.00832}{\lambda_0^2 - 0.036}, \qquad [3]$$

which for $\lambda_0 = 0.4416$ μm is $n = 1.645$. Rays exiting the lens at an angle i will be refracted by the resist surface and traverse the film at an angle r. If unrefracted rays incident at an angle i meet at a distance H_i below the air-resist surface, the refraction causes the rays to be brought to focus at a distance H_r below the resist surface,

$$H_r = H_i (\tan i / \tan r). \qquad [4]$$

Our apertured beam, upon passing through the lens, has marginal rays (those intercepting the local FWHM circumference) traveling at an angle $i = 22°$. From Snell's law, the angle r in the photoresist is found to be 13°. From Fig. 8, the observed value of H_i is found to be 2.35 μm. From Eq. [4], we find $H_r = 4.05$ μm, which is in reasonable agreement with the 4.9-μm thickness of the film that was more accurately determined by analyzing the interference fringes in its reflectivity-versus-wavelength spectrum, where the wavelength dependence of the index is assumed to be given by Eq. [3].

The magnitude of the peaks seen in Fig. 8 provides information about the absorption properties of the photoresist during exposure. We note that the bare-copper data of Fig. 8 provides an absolute reflectivity reference. The normal amplitude reflection coefficient

at the boundary between material of (complex) index of refraction n_1 and that of (complex) index of refraction n_2 is given by

$$S = (n_2 - n_1)/(n_2 + n_1). \quad [5]$$

In the case of copper at a wavelength of 4416 Å, the complex index is found from Heavens[6] to be

$$n(\mathrm{Cu}) = 0.87 + 2.2j. \quad [6]$$

The power reflection coefficient R at the boundaries of interest can be calculated directly as the absolute square of S determined from Eq. [3], with the results that R(air-Cu) = 58.4%, R(air-resist) = 5.9%, and R(resist-Cu) = 48.7%. From the measured relative peak heights of Fig. 8, we can calculate the power absorption coefficient α_P defined by

$$P(z) = P(O) \exp(-\alpha_P z), \quad [7]$$

where P(O) is the power entering the film, $P(z)$ is the transmitted power, and z is the path length through the film. The results of these calculations are that α_p(fully bleached) = 0.11/μm, α_p(unexposed) = 0.23/μm, and α_p(record) = 0.13/μm.

The result for the fully bleached case is consistent with the data of Kaplan and Meyerhofer,[7] adjusted to compensate for the differences in concentration of sensitizer in the films. Our value of the absorption constant for the unexposed case is significantly higher than their value, which for 4416 Å was essentially unchanged from the bleached case. For the unexposed, resist, the 4416 Å line lies on a very strong absorption edge which can be shifted in wavelength by processing. Their film was of pure sensitizer, while our resist has only 12% sensitizer, so such a disagreement is not surprising. The decrease of the reflectivity by the upper surface upon bleaching is reproducable and too large to be accounted for by changes in the published bulk properties (index of refraction and absorption) with bleaching.

4.5 Laser Power and Alignment

The laser power to the resist surface is controlled by the position of a motor-driven neutral-density wedge attenuator and the incident power is monitored by a photodetector. During test recordings, power and focus are varied in order to insure that the proper conditions for good grooves are obtained somewhere on the recording. Since we also require that the average slope of the groove walls be

vertical, care must be taken to insure that the incident laser beam is perpendicular to the photoresist. Beam splitter No. 2 can be rotated and translated to accomplish this final adjustment. Unfortunately, because the beam that is reflected off the substrate can be reflected again by other optical surfaces in the system, it is difficult to duplicate the exposing beam geometry unless the substrate is actually in place. When it is in place, we can no longer measure the light distribution. Thus, to see that the final tilt adjustment has been made properly, we must make a series of test recordings into the photoresist while varying the translation and tilt of beam splitter No. 2 and then evaluate the resulting grooves to establish optimum settings for these controls. Once a convenient developer and development time have been chosen, the development is always done with a constant developer composition and for a fixed time.

Perhaps the most frustrating aspect of the recording/developing process is its nonreproducability. We have attempted to minimize this nonreproducibility by coating all substrates of a set in a single morning and exposing and developing them under nominally identical conditions. Despite this attempt to maintain constant coating conditions, exposure conditions, and development conditions, the development rate still varies significantly from recording to recording. Thus, to stand a reasonable chance of transferring a given groove profile observed on a test recording to a production substrate of the same set, several production recordings must be made.

The He-Cd laser is polarized, and this aspect is utilized to prevent feedback of power into the laser cavity, which would cause unwanted oscillations in the laser power. The isolation of the laser is accomplished by inserting a polarizer and a quarter-wave plate in the laser beam before it enters the variable attenuator. The polarizer is oriented to pass the incident laser light; the quarter-wave plate converts this to circularly polarized light on the first pass; and then the return beam is converted back to linearly polarized light whose plane of polarization has been rotated by 90 degrees with respect to the original polarization direction. This reflected beam is then blocked by the polarizer.

4.6 Recorder Mechanics

The recorder turntable consists of a 15-inch-diameter aluminum plate mounted on a spindle supported by an air bearing. The spindle also incorporates the rotor for a dc motor. The motor housing is mounted on a machine slide equipped with a 10-turns-per-inch (TPI) lead screw. This screw is driven by a dc motor through a 100:1

speed-reducing worm gear. A microscope with an auxiliary capacitance sensor rigidly attached is swung over the substrate when the turntable slide is in the load position. The top surface of the substrate is brought up to a fixed height, and the surface is leveled by adjusting 6 vertical 100 TPI leveling screws until the capacitance sensor indicates that, upon slow rotation of the substrate, the surface is everywhere at the proper height to better than 2.5 μm vertical runout. Centering is accomplished by adjusting horizontal 100 TPI screws located on three of the leveling pads. The centering accuracy is measured by slowly rotating the substrate while viewing, through the microscope, a single circular groove that was mechanically cut into the substrate surface after this surface was machined flat.

The turntable rotational and translational drive motors are both controlled by a voltage that is proportional to the inverse of the radius. The required control signal is derived by supplying a linear potentiometer with a fixed voltage, coupling the potentiometer slider to the radial motion of the turntable, and using the output from the slider to drive an operational amplifier. The op-amp output is applied to the denominator input terminal of an analog divider, and a fixed reference voltage is applied to the numerator input terminal. By this method, we can obtain a control voltage that can generate constant linear velocity and constant pitch spiral to an accuracy of a few percent.

5. Photoresist Development

After exposure, the substrate is washed with freon and spin-dried to remove any traces of grease or other airborn contamination. The substrate is mounted face-up on a slowly rotating turntable, and a rubber collar is placed around the edge to form a shallow pan. Approximately 600 cm^3 of developeer is poured onto the surface, filling the pan to a depth of 1 cm.

The speed of the process of development depends on the developer used and on how much laser energy the photoresist has been exposed to locally. Initial tests indicated that contact of the photoresist with full strength Shipley AZ developer for 180 seconds would produce grooves of approximately 2.4 μm width down to the substrate when the resist is previously exposed locally to somewhat less than the full available focused laser power at a scan velocity of 300 cm/sec. Thus, these development conditions (Shipley AZ developer, 180 seconds) were established as our standard, and fine changes in groove width are accomplished by changing the laser power slightly.

After development, the substrate is washed with deionized water and baked.

6. Groove-Profile Evaluation

As indicated earlier, because of the dimensions of the grooves involved, the detailed experimental evaluation of the exposure/development process can only be made using a scanning electron microscope (SEM). As this instrument requires a conductive sample, the photoresist relief pattern must first be converted into a metal replica. This is accomplished by evaporating a 1200 Å thick gold layer over the entire surface of the test substrate and then electroplating a 0.005-inch-thick layer of nickel onto this gold film to form a thin master. The metal master is easily separated from the substrate at the resist layer, and acetone can be used to remove the residual photoresist from the master. The SEM can easily resolve features much smaller than the dimensions of the replicated grooves, but because the groove walls are smooth in the tangential direction, a fiducial viewing line must be provided to enable us to visualize the groove profile. Two methods of generating such a line, which corresponds to the intersection of a radial plane (normal to the disc surface) with the replica surface, are described in the subsections below.

6.1 Contamination Line Profiles

The simpler method, used for quick surveys of test recordings, involves punching a 0.5-inch-diameter disc from the master, mounting it in the SEM, pumping the system down to $\sim 10^{-4}$ Torr pressure, and making multiple scans across a groove along a single path with a small-diameter electron beam. This SEM beam locally heats the sample, and contaminants in the vacuum system collect on the sample surface along this line. When the SEM scan is shifted back into the raster-scan viewing mode, the contamination line stands out in sharp contrast to the rest of the surface. The sample can now be rotated almost 90° so as to cause the plane of the contamination line to be presented almost perpendicular to the beam. In this orientation, the contamination line represents a profile of the groove that can be photographed and measured.

Fig. 9 gives results of this procedure for grooves generated using a constant laser power under four different focus conditions: Fig. 9a is for laser focus (beam waist) 0.6 μm above the photoresist-copper interface; Fig. 9b corresponds to laser focus approximately 1.9 μm

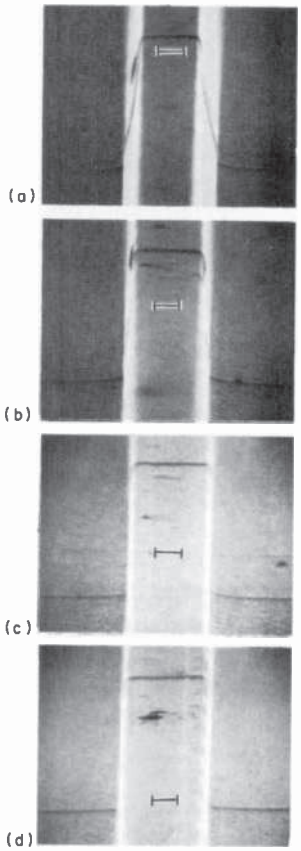

Fig. 9—Contamination-line views of replica of grooves generated by a focused beam with focal plane at the positions indicated by the black horizontal line. The length of the black horizontal line corresponds to the diameter of the incident beam waist which is 0.91 μm (FWHM). The depth of the groove in each case is 4.7 μm.

away from that surface; Fig. 9c to focus 3.1 μm up from the copper; and Fig. 9d to focus at 4.4 μm up, i.e., almost at the top surface. The head-on contamination line photograph of Fig. 9a for the focus near the bottom surface of the photoresist shows a strongly tapered nonreentrant groove profile. In Figs. 9c and 9d, the contamination line disappears along the sidewalls, and we can only guess what the corresponding groove profiles are.

We can, however, generate a contamination line groove profile in these cases by tilting the sample about a tangent to a groove so that the bottom, top, and one face of each groove are exposed to the

contaminating beam. An SEM photograph for that face is then taken by tilting the sample about both a radial and a tangential axis. Figs. 10a, 10b, 10c, and 10d were made in this manner to display the profile of the face of the groove nearest the substrate center. This complete procedure was repeated again to generate the photographs of Figs. 11a, 11b, 11c, and 11d, which show the face nearest the outside radius. From such a set of photographs, it is possible to obtain information that is adequate to establish where the optimum focus position is. However, because it is extremely difficult to set up angles in the SEM precisely, both for the contamination line scans and for the subsequent viewing, and because there are inherent distortions in the SEM scan, the technique described above is inadequate to establish groove tilt to the 1° reso-

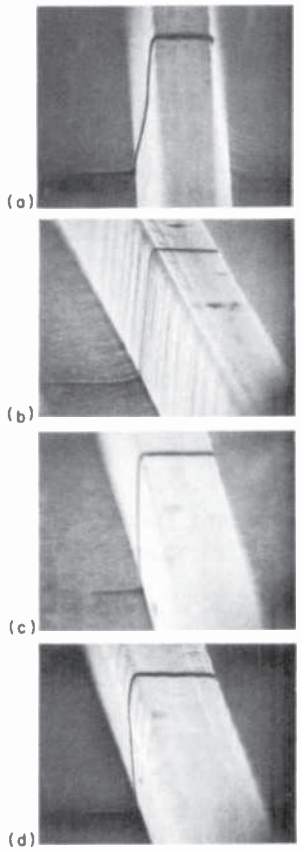

Fig. 10—Contamination line view of side of groove face nearest center of disc for grooves corresponding to those of Fig. 9.

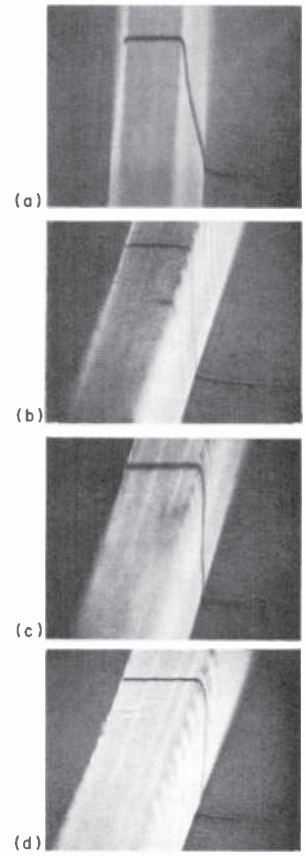

Fig. 11—Contamination line view of side of groove face nearest outer radius for grooves corresponding to those of Fig. 9.

lution required. To circumvent these limitations, the method described below for precise evaluation of the groove profile was developed.

6.2 Cross-Sectioned Samples

This second method of groove profile evaluation consists of cutting a small radial strip from the gold-covered nickel master, electroplating a few mils of nickel onto this gold layer, and then standing this strip on edge with the radius horizontal. The sample is potted in epoxy and allowed to cure. It is sawed, again along a radius, and the sawed surface is polished to present an edge view of the grooves. The polished surface is then etched with a gold etching solution

that does not attack the nickel. The polished surface is thus transformed into a deep relief structure in which the groove profile is easily seen using an optical microscope and can be accurately measured using a scanning electron microscope.

In Fig. 12 we see explicitly the groove profiles corresponding to the four focus conditions described for Figs. 9, 10, and 11. Note that a single head-on view now gives us the complete profile, even for the case of re-entrant grooves. A study of the re-entrant grooves on the test master is useful to establish focus and groove tilt, but a metal part containing grooves of this shape could not be replicated without damage during separation. Notice also the hole clearly vis-

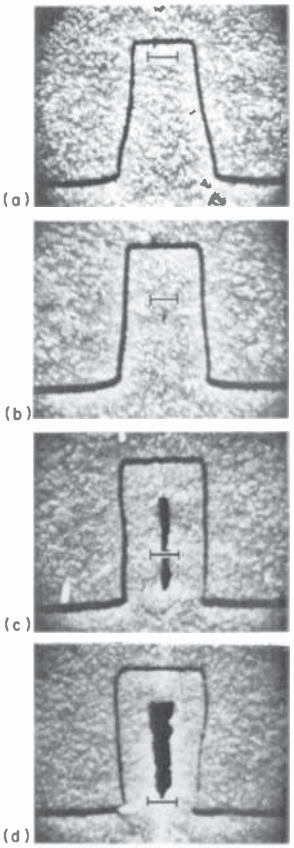

Fig. 12—Sectioned profiles of the grooved replica described in Fig. 9. Again, the position of each horizontal line corresponds to the focal plane of the incident laser beam and its length corresponds to the diameter of the beam waist of 0.91 μm (FWHM).

ible in the center of Figs. 12d and 12c and just visible in 12b. For a re-entrant structure, a conformal electrodeposition will produce such a void. In the real case, the deposition usually occurs more rapidly at sharp edges (that are sticking into the bath), so that deep and narrow vertical walled structures, or even slightly tapered ones, can also be expected to generate these voids.

Figs. 9–12 show one major effect of the change in focus for one particular laser power, collimating-lens focal length, photoresist thickness, and substrate reflectivity. An experimental determination of an large number of groove shapes for various possible combinations of the above variables would obviously be extremely tedious. For this reason and in order to more fully understand the exposure/development process, we have developed a theoretical model to explore the range of parameters relevant to keel-lap mastering. The purpose of this analysis is to provide some guidance for experimental efforts. The basic physical/chemical aspects of deep resist recording are not sufficiently understood to allow the use of the model developed here for the precise specification of the process parameters that produce a desired relief pattern, but it does yield useful information about how the recording and development parameters affect the shape of the relief surface.

7. Theoretical Model

The etch model used as the basis for our calculations assumes (a) that the exposure is via a Gaussian beam scanned uniformly across the surface, (b) that local etching proceeds normally to the etch boundary, and (c) that the evolution of the boundary can be adequately described by the numerical integration of a set of difference equations. Each of these aspects is discussed in some detail below.

7.1 Laser Exposure Pattern

The incident beam inside the resist layer is assumed to be described in regions away from the focal plane by the more complete Gaussian expression

$$E_I(\rho, z) = A_I \frac{w_0}{w(z)} \exp\left(\frac{-\rho^2}{w^2(z)} + j\,\phi(\rho, z)\right). \qquad [8]$$

Here $E_I(\rho,z)$ is the field amplitude described in terms of a cylindrical coordinate system, $\rho = \sqrt{x^2 + y^2}$; A_I is the amplitude normalization constant; $\phi(\rho,z)$ is the phase function; w_o is the beam waist;

$$w(z) = w_0 \sqrt{1 + (z/z_0)^2}; \quad [9]$$

z is the distance from the waist along the beam direction;

$$z_0 = \pi w_0^2/\lambda; \quad [10]$$

and λ is the wavelength of the exposing light in the photoresist. The phase function $\phi(\rho,z)$ can be shown to be[8]

$$\phi(\rho,z) = k\left(z + \frac{\rho^2}{2z[1 + (z_0/z)^2]}\right) - \text{arc tan}\left(\frac{z}{z_0}\right), \quad [11]$$

where $k = 2\pi/\lambda$. The positions $z = 0$ and $z = z_a$ are, respectively, the positions of focus and the air-resist interface. The effect of absorption of the resist can be accounted for by an amplitude absorption coefficient α_A. The field amplitude is thus reduced as it progresses through the resist according to

$$A_I = A_0 \exp[-\alpha_A (z - z_a)]. \quad [12]$$

We now assume that the resist is coated onto a partially reflecting substrate located at $z = z_R$ and having a (complex) reflection coefficient S. The reflected field configuration is simply obtained by making the reflection transformation substitution where z goes to $z' = 2z_R - z$ and noting that $A_R = A_I(z')S$. We then have, for the reflected field,

$$E_R(\rho, z) = E_I(\rho, z')\, S. \quad [13]$$

For the typical recording arrangement, if we assume that the substrate is moved uniformly across the beam in the y direction, the total local exposure $D(x,z)$ is found from

$$D(x, z) = \eta \int_{-\infty}^{\infty} dy\, |E_I + E_R|^2, \quad [14]$$

where η is a constant proportional to the dielectric constant of the resist and is inversely proportional to the velocity. If the integration indicated in Eq. [14] is performed, the result can be conveniently written as the sum of three terms D_I, D_R, and $D_{I,R}$ due, respectively, to the incident, reflected, and interfering fields. Thus

$$D(x, z) = D_I + D_R + D_{I,R}, \quad [15]$$

where

$$D_I(x, z) = \eta \sqrt{\frac{\pi}{2}} A_i^2 \frac{w_0^2}{w(z)} \exp\left(-2\alpha_A (z - z_a) - \frac{2x^2}{w^2(z)}\right), \quad [16]$$

$$D_R(x, z) = |S|^2 D_i(x, z'), \quad [17]$$

$$D_{I,R}(x, z) = \eta G(z, z') \frac{2\sqrt{\pi} \exp(-x^2 g_1)}{(g_1^2 + k^2 g_2^2)^{1/4}} \cos\{\zeta\}, \quad [18]$$

with the auxiliary expressions

$$G(z, z') = |S| A_I^2 \frac{w_0^2}{w(z)w(z')} \exp(-2\alpha_A (z_R - z_a)), \quad [19]$$

$$g_1 = \frac{1}{w^2(z)} + \frac{1}{w^2(z')}, \quad [20]$$

$$g_2 = \left(\frac{z}{w^2(z)} - \frac{z'}{w^2(z')}\right) \frac{w_0^2}{2z_0^2}, \quad [21]$$

$$\zeta = k(2z - 2z_R + x^2 g_2) + \delta - \Phi, \quad [22]$$

$$\delta = \arctan\left(\frac{kg_1}{g_2}\right) + \arctan(z/z_0) - \arctan(z'/z_0). \quad [23]$$

Here ϕ is the phase factor of the amplitude reflection coefficient S.

7.2 Local Etching

We assume that the local etching proceeds normal to the surface contour. The local etch rate (for given resist and developer formulations) is a function $F(x,z)$ of only the local total exposure $D(x,z)$. The etch velocity, $\mathrm{V}(x,z)$ is then a vector which is locally of the form

$$\mathrm{V}(x, z) = F(x, z)\, \mathrm{n}(x, z), \quad [24]$$

where $\mathrm{n}(x,z)$ is the unit vector normal to the surface. The most commonly employed models for etching assume one of the three following forms:

$$F1(x, z) = C_1 + C_2 D(x,z) \quad [25]$$

$$F2(x, z) = C_1 \exp(C_2 D(x, z)) \quad [26]$$

$$F3(x, z) = C_1 + C_2 D^{\gamma}(x, z). \quad [27]$$

It is convenient to refer to the functions $F1$, $F2$, and $F3$ respectively, as the linear-with-erosion, exponential, and power-law model etch rates. In Eqs. [25] through [27], C_1 describes the erosion rate, i.e., the etch rate at zero exposure, and C_2 is the exposure normalization constant.

7.3 Numerical Integration Procedure

The evolution of the resist–developer interface contour is traced by converting Eq. [24] to a set of difference equations that are numerically integrated. To do this, we divide the contour at time T into a number of segments whose end points are labeled by the integer N. The positions of the N points are chosen such that each of the N points is (straight line) equidistant from its nearest neighbors. The normal to the contour at point N is taken to be the normal to the line joining points $N - 1$ and $N + 1$. The difference equation form of Eq. [24] is then used to determine the position of each of the end points at time ΔT later. The new set of points is used to define a smooth curve using a standard spline routine. The spline routine requires a knowledge of the slopes of the curve at the end points, and in most real situations this can be done by selecting the end points in regions of negligible exposure where the slope is the initial slope of the air–resist interface. The procedure for dividing this new contour into the same number of equal segments is then repeated, and the motion of the new end points during the next time interval ΔT is again calculated from the difference equations.

7.4 Results of Computer Calculations

Extensive computer calculations were done using the linear, linear-with-erosion, and exponential models of photoresist development. For the linear model, $C_1 = 0$ and the single constant C_2 was chosen to obtain the observed development rate at the center of the beam of 3.0 μm/minute. In the case of the linear-with-erosion and exponential models, the constants C_1 were chosen to give the observed erosion rate of 0.05 μm/minute. The constant C_2 in the exponential model was then adjusted to obtain the observed etch rate at the center of the beam. The results of some of these calculations are displayed as Figs. 13, 14, 15, and 16.

The calculations for Fig. 13 assume zero absorption in the photoresist layer and an amplitude reflection coefficient at the photoresist–copper boundary of 0.7. Fig. 13 illustrates, using the linear model without absorption, the effects of beam-waist size and focal position on the evolution of the groove. The heavy horizontal line in each figure is located in the focal plane and the vertical bar at its end indicates the position of the half-power beam-waist radius (FWHM/2) for the incident beam. In going from top to bottom of

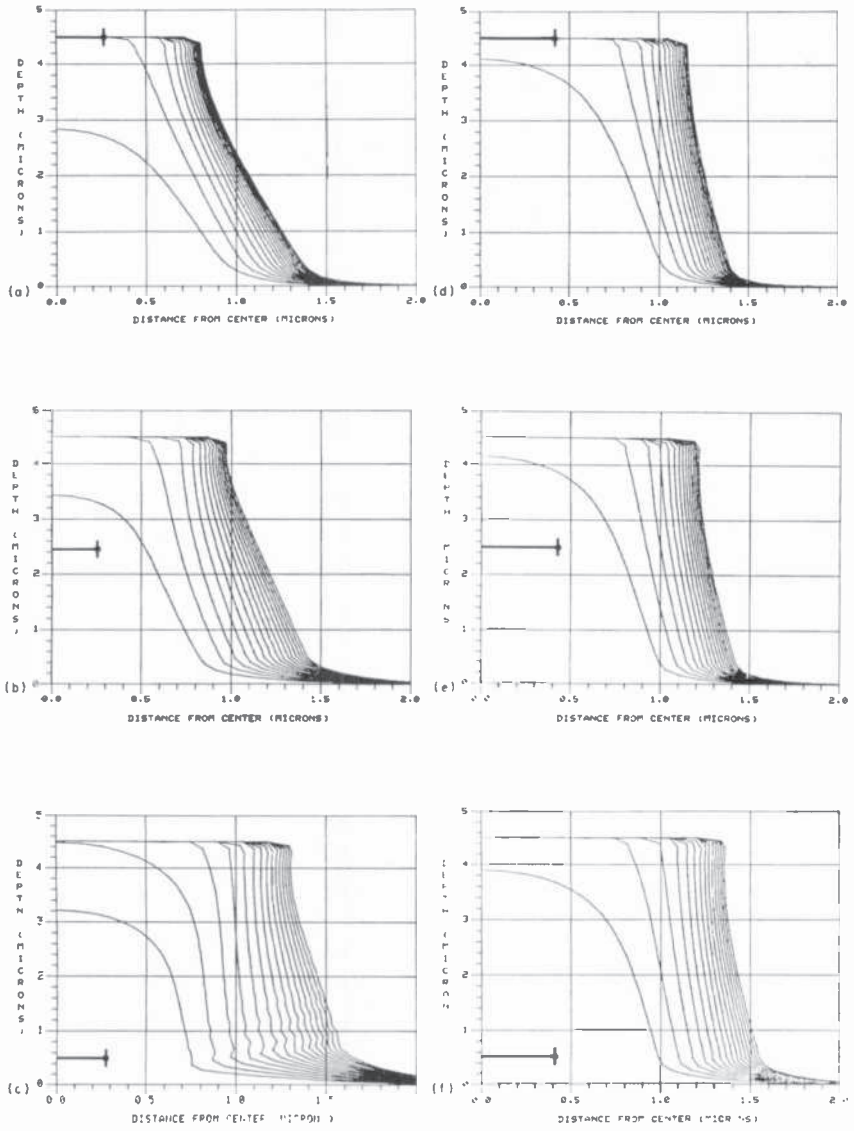

Fig. 13—Effect of focal position and spot size on the evolution of the grooves during development. The computer calculations used the linear-model, zero resist absorption, and an interface amplitude reflectivity of 0.7. Times shown are 1 to 8 minutes at 0.5 minute intervals. The vertical position of the dark horizontal line indicates the input-beam focal plane while the horizontal position of the end marker indicates the input-beam waist radius (FWHM/2). Note the foreshortened vertical scale.

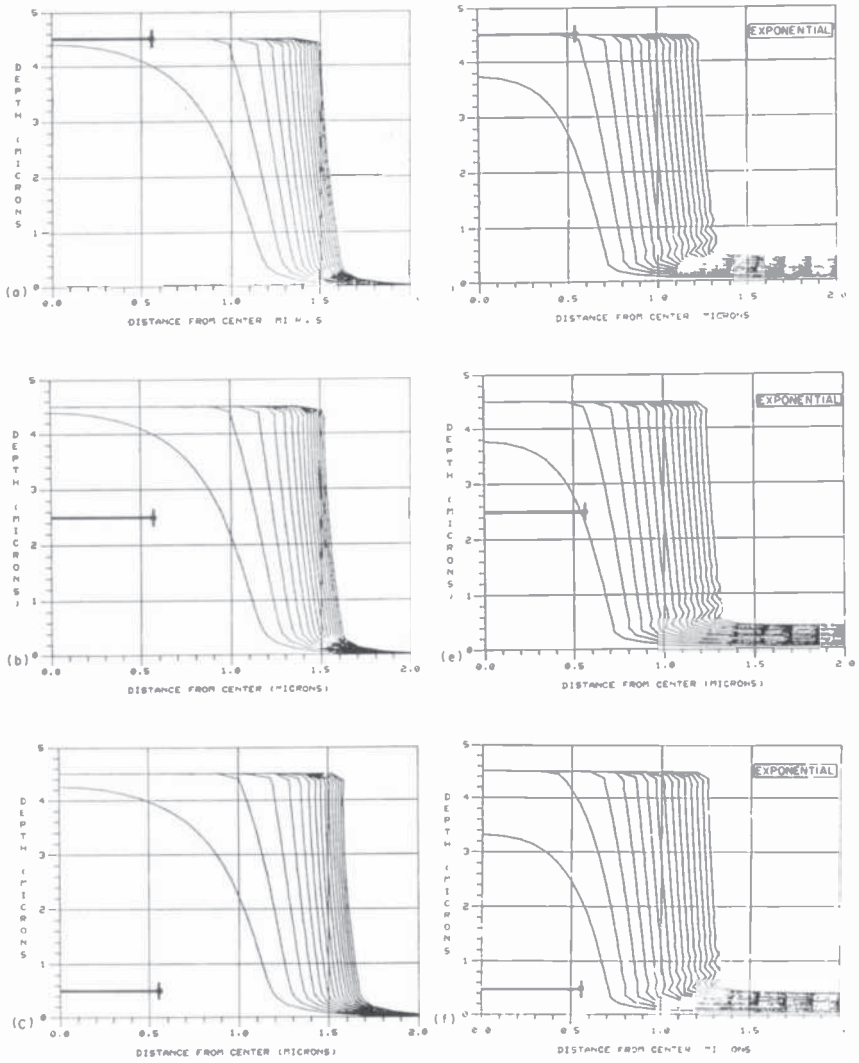

Fig. 14—Effect of focal position and model on the evolution of the grooves. Computer calculation uses linear model for (a), (b), and (c) and the exponential model for (d), (e), and (f). Zero resist absorption and an interface amplitude reflectivity of 0.7 are assumed. Times shown are 1 to 8 minutes at 0.5 minute intervals. The vertical position of the dark horizontal line indicates the input-beam focal plane, while the horizontal location of the end marker indicates beam waist radius (FWHM/2). Figs. 14 (a), (b), and (c) can also be considered as an extension of Fig. 13 to a larger beam radius. Note the foreshortened vertical scale.

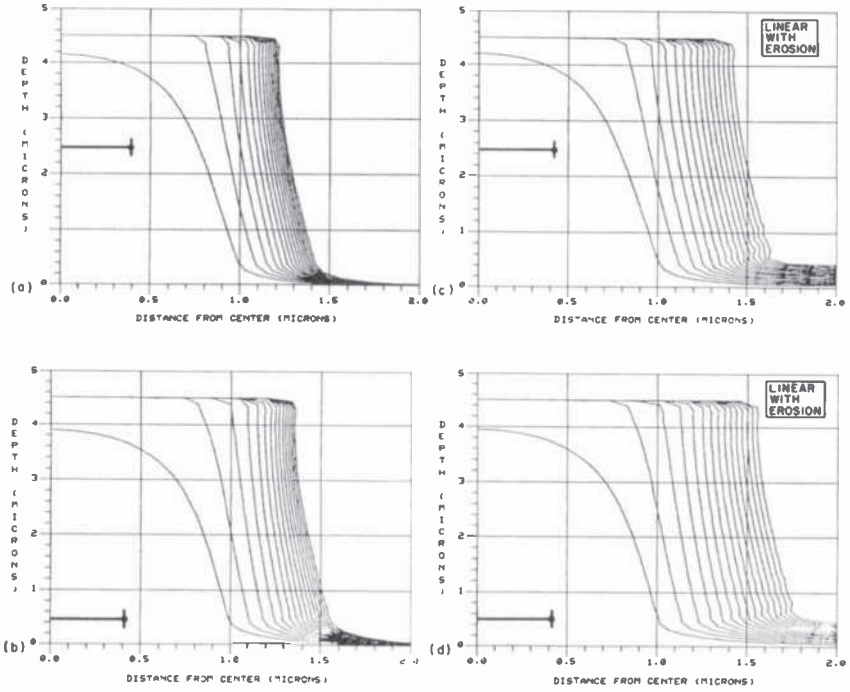

Fig. 15—Effect of focal position and erosion on the evolution of the grooves. Computer calculation uses linear model for (a), (b), and (c) and the linear-with-absorption model for (d), (e), and (f). Zero resist absorption and interface reflectivity of 0.7 are assumed. Times shown are 1 to 8 minutes at 0.5 minute intervals. The vertical position of the dark horizontal line indicates the input-beam focal plane, while the horizontal position of the end marker indicates the input-beam waist radius (FWHM/2). Note the foreshortened vertical scale.

Fig. 13, we notice the strong effect of changing focus on the groove shape, which is consistent with our experimental observations.

In Figs. 14a, 14b, and 14c, we extend the linear model to a larger spot size. Figs. 14d, 14e, and 14f present the results of calculations using the exponential model. Aside from reducing the overall groove height, the use of the exponential model calculations are not significantly different than those using the linear model. For designing optimum recording conditions, however, the linear model is probably more appropriate, because the exponential model is likely to over-estimate the effect of photoresist nonlinearities.

Similarly, Fig. 15 shows a side-by-side comparison of the results

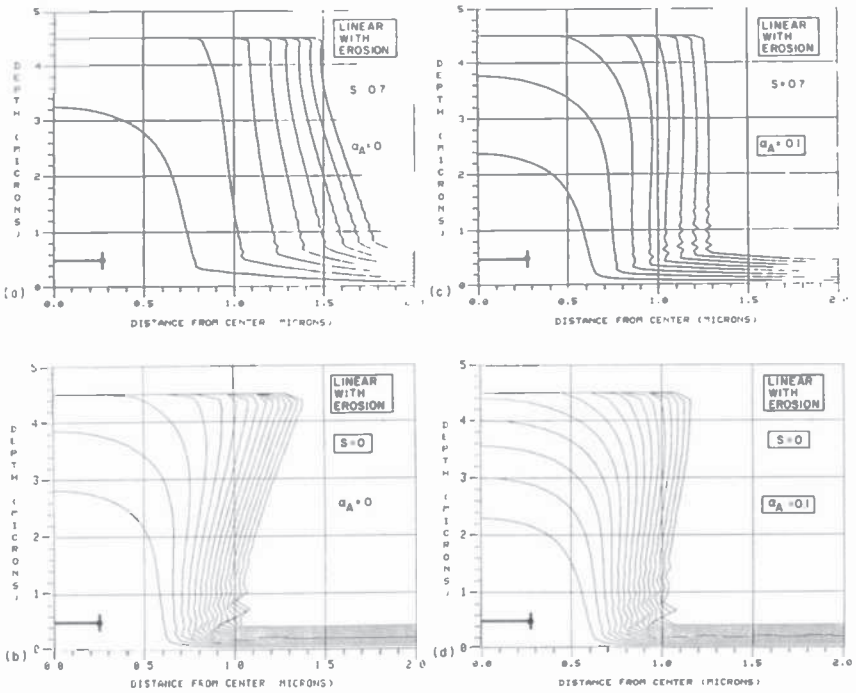

Fig. 16—Effect of changes in resist absorption and/or resist–copper interface reflection on the evolution of the grooves. The calculations were made with (a) $S = 0.7$, $\alpha_A = 0$; (b) $S = 0$, $\alpha_A = 0$; (c) $S = 0.7$, $\alpha_A = 0.1$; and (d) $S = 0$, $\alpha_A = 0.1$. Times shown for (a) and (c) are 1 to 8 minutes at 1.0 minute intervals; for (b) and (d) are 1 to 8 minutes at 0.5 minute intervals. The vertical position of the dark horizontal line indicates the input-beam focal plane, while the horizontal position of the end marker indicates the input-beam waist radius (FWHM/2). Note the foreshortened vertical scale.

of model calculations, this time for the linear model with and without erosion. Again, with the trivial exception of the reduction of the overall groove height by the linear-with-erosion model, the particular model used does not significantly effect the qualitative behavior of the groove evolution during development.

In Fig. 16 we show explicitly how absorption by the photoresist and reflectivity at the photoresist-copper interface affect the evolution of the groove profile. The beam diameter and focal position are that of Fig. 13c, which is reproduced as Fig. 16a. The effects of changing the absorption, the interface reflectivity, or both are dramatically demonstrated.

None of these calculations include the interference term of Eq. [18] explicitly, but since it is an oscillatory function whose average value is zero, the effect of neglecting this term would only be noticed if the calculations were carried out on a very small scale. Since we have often noticed the strong interference pattern that is etched into the resist walls, as can be seen in Figs. 9b, 10b, and 11b, some computer calculations seemed justified. To include such effects, however, the spatial grid of the numerical calculations must be made much finer, and when this is done the computer cost goes up rapidly. Thus only small development times were explored, and these did show the evolution of fringes spaced at approximately one half the exposure wavelength (in the resist).

Thus we see that a fine balance must be maintained between many contributing factors to enable us to generate grooves of the required profile. Note also from the theoretical curves that not only the width but also the shape is critically affected by development time as well as by the other parameters discussed.

Acknowledgments

The authors wish to acknowledge the special efforts of the following members of the Laboratory staff. The original idea for machining the stylus tips in the shape of a keel is due to E. O. Keizer. The original keel-lap recorder was assembled and early recordings were made by A. H. Firester, J. P. Russell, and M. E. Heller, with the assistance of C. B. Carroll in the mechanical design and construction. W. C. Henderson assisted with or made hundreds of test recordings. K. F. Etzold and D. W. Thompson have contributed significantly in many areas of the keel-lap effort including the development of the sectioning technique. A. Sabo has admirably handled all of the resist processing. All of our experimental views of the grooves are the result of painstaking effort by the SEM analysis group: J. H. Reisner, W. L. Lees, Jr., W. R. Campbell, 3rd, and R. E. McCoy. P. V. Valembois and E. J. Holub provided the finely machined substrates. Numerous discussions with G. Kaganowicz concerning specifications of the optimum lapping-groove profiles and with H. Scheible on resist processing techniques are gratefully acknowledged. M. Kaplan and D. Meyerhofer provided all resist-related data and were helpful with numerous discussions relating to the physical model of resist etching. Much of the computational algorithm is the result of suggestions made by R. W. Klopfenstein. System programming assistance was provided by A. W. Jessup, Jr.

References:

[1] E. O. Keizer, Keel-Tipped Stylus for VideoDisc System, U.S. Patent No. 4,162,510, July 24, 1979.
[2] A. H. Firester, C. B. Carroll, I. Gorog, M. E. Heller, J. P. Russell, and W. C. Stewart, "Optical Readout of the RCA VideoDisc," *RCA Rev.*, 39(3), p. 392, Sept. 1978.
[3] M. Born and E. Wolf, *Principles of Optics,* Fifth Edition, Pergammon Press, (1975), p. 395.
[4] P. Jacquinot and M. B. Roizen-Dossier, "Apodization," *Progress in Optics*, John Wiley & Sons, N.Y. (1963), p. 31.
[5] M. Kaplan, private communication.
[6] O. S. Heavens, *Optical Properties of Thin Solid Films,* Dover Publications, Inc., New York (1965), p. 200.
[7] M. Kaplan and D. Meyerhofer, "Response of Diazoquinone Resists to Optical and Electron-Beams Exposure," *RCA Rev.*, 40(2), p. 166, June 1979.
[8] H. Kogelnik and T. Li, "Laser Beams and Resonators," *Proc. IEEE,* 54, p. 1312, (1966).